Invariant Forms of Dissolution Fingers

Stanisław Żukowski,[1,2] Silvana Magni,[1] Florian Osselin,[3] Filip Dutka,[1] Max Cooper,[1] Anthony J. C. Ladd,[4] and Piotr Szymczak[1]

[1]*Institute of Theoretical Physics, Faculty of Physics, University of Warsaw, Pasteura 5, 02-093 Warsaw, Poland*
[2]*Laboratoire Matière et Systèmes Complexes (MSC), UMR 7057, CNRS & Université Paris Cité, 10 rue Alice Domon et Léonie Duquet, 75013 Paris, France*
[3]*Institut des Sciences de la Terre, Orleans, France*
[4]*Chemical Engineering Department, University of Florida, Gainesville, Florida 32611, USA*

(Received 3 April 2024; accepted 29 January 2025; published 4 March 2025)

Dissolution of fractured and porous media introduces a positive feedback between fluid flow and reactant transport, leading to the emergence of pronounced, fingerlike channels. We investigate the formation of these structures using a microfluidic Hele-Shaw cell with a soluble bottom. Our experiments show that the shape of dissolution fingers is invariant and reveals itself over time as the fingers extend into the system. By combining reactive-transport theory and conformal mapping techniques we derive these invariant forms. We relate these results to natural dissolution fingers in karst landscapes, and illustrate how to determine the groundwater flow rate responsible for their formation based on the finger shape.

DOI: 10.1103/PhysRevLett.134.094101

Climatic conditions can leave a permanent mark on the landscape in the shapes and forms left behind by geological processes. Geochemical transformations are an unusual class of pattern-forming systems, in that the pattern does not decay once the driving force is removed [1–3]. While mechanical erosion shapes river valleys and mountain ridges [4–7], chemical erosion shapes caves and karst towers, as well as smaller surface forms, such as grooves, rills, or solution pans [8–12]. An intriguing example of spontaneously forming dissolution structures are solution pipes [Fig. 1(a)]. These fingerlike channels are caused by the infiltration of limestone formations by rainwater, which has become acidic through the absorption of carbon dioxide from the atmosphere and soil [13,14]. Such pipes are abundant in nature and often have regular forms, suggesting that they might represent invariant asymptotic forms of reactive-transport processes. In this Letter, we report theoretical and experimental evidence of an underlying time-invariant form for dissolution fingers, which reveals itself during the growth process.

The existence of invariant solutions is a compelling characteristic of many unstable growth processes, particularly since the early stages are often characterized by a chaotic sea of fingerlike structures [15,16]. And yet, in the longtime limit, the pattern often simplifies, with the appearance of invariant growth forms which advance into the system without changing their shape. A well-known example is the Saffman-Taylor finger, which emerges as an asymptotic solution in viscous fingering [17], or the Ivantsov paraboloid [18], which is the corresponding solution in solidification. Other examples include the regular shapes of flames [19] or crystals growing in a capillary [20]. In natural systems, a similar concept was used to describe stalactites [21], icicles [22,23], karst pinnacles [24] and travertine cones [25].

The importance of these invariant solutions lies in their independence from the initial conditions; the ideal shapes attained in the longtime limit are characterized by a small number of parameters, which record the physical conditions under which the growth occurred. For example, the width of a Saffman-Taylor finger is linked to the capillary number (involving viscosity, flow rate, and surface tension) [17], whereas the invariant shape of a crystal growing in a capillary is a function of solution supersaturation [20]. Our aim is to find a similar connection for dissolution fingers, which should enable us to obtain paleoenvironmental or even paleoclimatic data from the period in which they were formed.

Arguably, the simplest system in which to study dissolution instabilities is a Hele-Shaw cell with a soluble

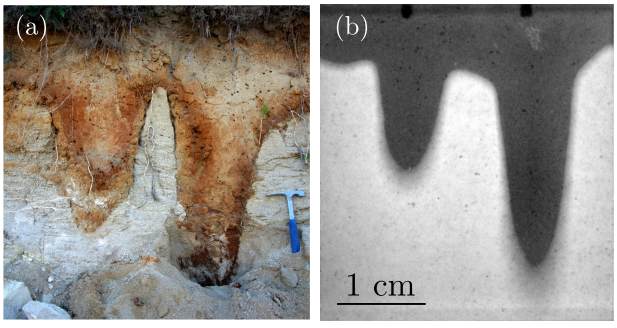

FIG. 1. (a) Solution pipes in limestone bedrock (Smerdyna, Poland). (b) Dissolution fingers formed in a microfluidic system.

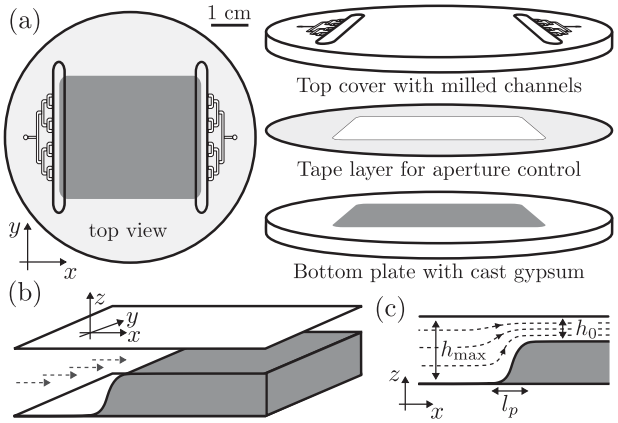

FIG. 2. The experimental setup. (a) The chip is a three-layer sandwich. The top polycarbonate plate has two networks of microfluidic channels: the inlet, delivering a uniform flow of fresh water into the system, and the outlet, draining fully saturated water. The bottom plate is flat, except for a shallow rectangular (3.3×3.8 cm) indentation filled with gypsum. The two plates are glued together by a double-coated tape, which at the same time introduces an aperture of thickness h_0. (b),(c) Fresh water flowing into the system (dashed arrows) gradually dissolves the gypsum, effectively introducing two phases: dissolved (with aperture h_{max}) and undissolved (h_0). The two phases are separated by a transition region with a characteristic length scale l_p.

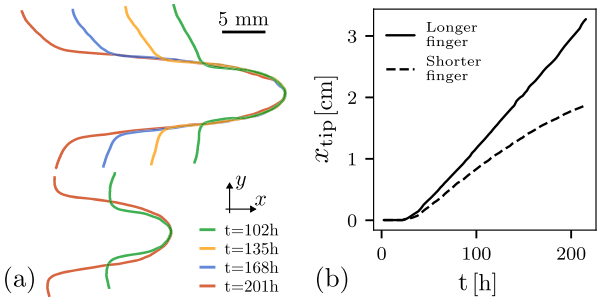

FIG. 3. (a) Outlines of the fingers, $x_f(y,t)$, from the experiment depicted in Fig. 1(b), captured at different moments of time and superposed at the tips. The body of the longer finger retains its shape once it has emerged. The experiment was conducted at a volumetric flow rate $Q_{tot} = 0.5$ ml/h, $h_0 = 210$ μm, and $h_{max} = 710$ μm. (b) The position of the tip versus time, $x_{tip}(t)$.

bottom. A classical Hele-Shaw cell consists of two closely spaced flat plates with a small gap between them [Fig. 2(a)]. The average velocity in a thin film of liquid within the cell is linked with the pressure gradient through the Darcy's law, $\boldsymbol{v} = -M\nabla p$, where the mobility $M = h^2/12\mu$, h is the gap between the upper and lower surface [Fig. 2(b)], and μ represents the fluid viscosity. The mobility can thus be changed in two different ways: either by changing the viscosity of the fluid (as in the classical Saffman-Taylor experiment) or by modifying the depth of the Hele-Shaw cell.

A variable depth can be achieved by replacing part of the bottom plate with a soluble gypsum chip, as illustrated in Fig. 2(a). Fresh water, injected by a syringe pump, dissolves the gypsum layer from the left, becoming saturated with calcium ions in the process. Gradually, the dissolved region (with aperture h_{max}) appears at the inlet side, while the rest of the system maintains its initial aperture (h_0), as illustrated in Figs. 2(b) and 2(c). The boundary between these two regions, initially planar, becomes unstable due to a reactive-infiltration instability [26,27]: if small perturbations appear in the dissolution front, the flow will increase locally due to the higher mobility. This increased flow carries an undersaturated solution deeper inside the system. As a result, small inhomogeneities tend to grow and transform into highly permeable, fingerlike flow channels, as depicted in Fig. 1(b), similar in shape to the natural solution pipes in Fig. 1(a).

To investigate the shape of such fingers, we performed microfluidic experiments, introducing small cuts in the gypsum layer near the inlet, to trigger the formation of fingers in those locations [Fig. 1(b)]. We conducted both two-finger and single-finger experiments: the former to quantify the interaction between the fingers, and the latter to capture the invariant shapes of individual fingers.

In the two-finger system (Fig. 3), the individual fingers compete strongly: the longer finger, offering the path of least resistance, captures an ever-increasing portion of the flow at the expense of the shorter one. Interestingly, even though the shorter finger begins to move more slowly as it loses flow, the longer finger does not accelerate [Fig. 3(b)], unaffected by the fact that it is focusing an increasing fraction of the flow injected into the system. This is fundamentally different from most models of fingered growth [28–30] which predict a speedup in the longer finger.

Equally striking is an analysis of the finger shapes. If we trace the boundaries of the fingers at different moments in time and superimpose them in such a way that their tips overlap, we observe that they have been tracing the same invariant shape from the outset [Fig. 3(a)]. Over time, an invariant part of the finger simply shifts in the flow direction, and an increasingly longer invariant finger emerges. Parametrizing the shape of the finger as $x_f(y,t)$ the invariance condition becomes

$$x_f(y,t_1) - x_{tip}(t_1) = x_f(y,t_2) - x_{tip}(t_2), \qquad (1)$$

where $x_{tip}(t)$ is the x position of the tip at time t. Intriguingly, this behavior is observed only in the longer finger. By contrast, the shorter finger does not maintain its shape; a close examination of Fig. 3(a) reveals that it becomes progressively wider as it slows down.

The emergence of invariant shapes can be studied in more detail in single-finger experiments, using a larger aspect ratio microfluidic cell (5 cm × 1 cm). The growing

fingers have a regular shape, becoming more elongated at higher flow rates (Fig. 5). To find the invariant shape theoretically, we start with the equations describing flow and reactant transport in a Hele-Shaw cell. The average velocity $\boldsymbol{v}(x, y)$, comes from a lubrication (narrow aperture) approximation to the Stokes equations:

$$\boldsymbol{v} = -\frac{h^2}{12\mu}\nabla p, \qquad \nabla \cdot (h\boldsymbol{v}) = 0, \tag{2}$$

where ∇ is a two-dimensional gradient operator. The transport of calcium ions in the aqueous phase is described in terms of their undersaturation c, which is the difference between the saturation concentration c_{sat} and the average Ca^{2+} concentration in the fluid film. The vertically averaged concentration field in the fully dissolved finger body is described by the two-dimensional transport equation

$$\nabla \cdot (h_{\max}\boldsymbol{v}c - Dh_{\max}\nabla c) = 0, \tag{3}$$

where D is the diffusion coefficient of the calcium ions. A more detailed derivation can be found in Supplemental Material (SM), Sec. I [31].

Since the widths of the fingers are large, the dissolution process is transport limited. The relevant parameter here is the Damköhler number $\mathrm{Da} = kW^2/Dh_{\max}$ [see Eq. (8) in the SM [31]], where k is the reaction rate constant, and W is the width of the system. In our experiments Da is of the order of 1000; it can be even larger in natural systems such as solution pipes, where the diameter can be of the order of 1 m. Large values of Da indicate that the dissolution reaction is very fast compared to ion diffusion across the finger, implying that the solution saturates essentially instantaneously as it crosses the reaction front separating dissolved and undissolved material. This corresponds to a Dirichlet condition $c = 0$ at the boundary of the finger, and allows us to approximate the finger evolution as a moving boundary (Stefan) problem; a schematic is shown in Fig. 4. The local growth rate of the finger is determined by the diffusive flux of ions at the boundary (see SM, Sec. III [31])

$$u_n(t) = -\alpha D\frac{h_{\max}}{h_{\max} - h_0}(\boldsymbol{n} \cdot \boldsymbol{\nabla} c)_\Gamma, \tag{4}$$

where $\boldsymbol{n}$ is the outward normal to the finger boundary Γ. The coefficient $\alpha = \nu_{\mathrm{m}}/(1-\varphi)$ converts the flux of ions into a dissolved volume; it is determined by the molar volume (ν_{m}) and the porosity (φ) of the soluble material.

Solutions of Eq. (3) are characterized by the dimensionless Péclet number, which is a measure of the relative importance of advective and diffusive transport, $\mathrm{Pe} = Q_{\mathrm{tot}}/(Dh_{\max})$, where Q_{tot} is the total volumetric flow rate entering the system [see Eq. (9) in the SM]; in our experiments, Péclet numbers are in the range 50–500. For large Péclet numbers the fingers are strongly elongated, with a small aspect ratio, $w'(x) = \mathrm{d}w/\mathrm{d}x \ll 1$. One can

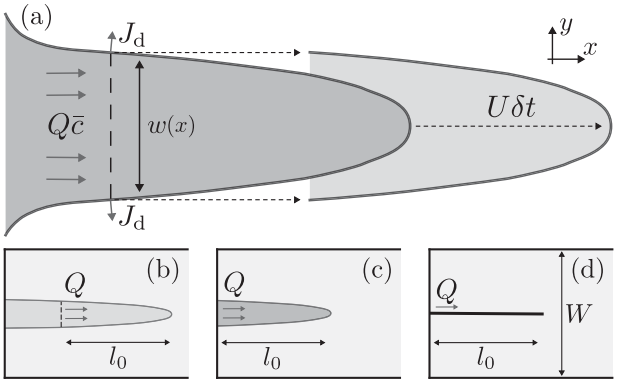

FIG. 4. (a) Schematic view of a single dissolution finger with a width profile $w(x)$, diffusive flux J_{d}, volumetric flow rate Q through the finger cross section, and total concentration flux $Q\bar{c}$ through the cross section. (b)–(d) Because of the invariance of the tip, the flow through a cross section located at distance l_0 from the tip of any finger (b), should be the same as the flow through the base of a finger of length l_0 (c). The total flow through the finger base is estimated analytically by approximating a finger with a thin line of the same length (d).

then assume that the flow rate and concentration profiles are locally analogous to those between the two parallel absorbing walls separated by distance $w(x)$. The flow is then simply a plug flow

$$\boldsymbol{v}(x, y) = \frac{Q(x)}{w(x)h_{\max}}\boldsymbol{e}_x + \mathcal{O}(w'(x))\boldsymbol{e}_y, \tag{5}$$

where $Q(x)$ is the total flow through the finger cross section at x. The problem of finding the concentration profile between two parallel absorbing walls is known as the Graetz problem [38], and for plug flow (5) the slowest spatially decaying mode is of the form [39]

$$c(x, y) = \frac{\pi\bar{c}(x)}{2}\cos\frac{\pi y}{w(x)}, \tag{6}$$

where axial diffusion has been neglected. In Eq. (6), $\bar{c}(x)$ is the average undersaturation in a cross section of the finger perpendicular to the direction of flow.

The flux of calcium ions within a cross section of the finger contains contributions from ion advection $Q\bar{c}$ and the diffusive fluxes, which are absorbed at the finger boundary, $J_{\mathrm{d}}(x) = -Dh_{\max}\boldsymbol{n} \cdot \boldsymbol{\nabla} c$ [Fig. 4(a)]. The latter can be approximated as $J_{\mathrm{d}}(x) = -Dh_{\max}\partial_y c$ by neglecting terms $\mathcal{O}(w'(x))$, as in Eq. (5). For steady state transport these fluxes balance:

$$(Q\bar{c})' = -Dh_{\max}\bar{c}\frac{\pi^2}{w}. \tag{7}$$

Next, we make use of the observation that the emerging body of the finger keeps its shape and translates only [Eq. (1)]. Points along the boundary move with the same x

velocity U, which is linked with the normal growth rate (4) by $u_n = Un_x$. In particular, this means that downstream of any cross section, the total volume of gypsum dissolved over time δt is $U(h_{\max} - h_0)w(x)\delta t$. This must be proportional to the incoming number of ions $Q\bar{c}(x)\delta t$ with proportionality constant α (Fig. 4):

$$U(h_{\max} - h_0)w = \alpha Q\bar{c}. \tag{8}$$

The volumetric flux inside a finger of length l, $Q(x, l)$, is constrained by the observation that the shape of the finger, starting from its tip ($x_{\text{tip}} = l$), remains the same during its evolution. This identity in shape implies that the flow field should also remain unchanged (SM, Sec. III [31]); thus $Q(x, l)$ should be a function of the distance from the tip only $Q(x, l) = Q(x_{\text{tip}}(t) - x)$. In particular, as shown in Figs. 4(b) and 4(c), the total flow through the base ($x = 0$) of the finger of length l_0, $Q(0, l_0) \equiv Q_0(l_0)$, should be the same as the flow at the cross section $x = x_{\text{tip}} - l_0$ of the same finger, captured at the later time

$$Q(x_{\text{tip}}(t) - l_0) = Q_0(l_0). \tag{9}$$

To calculate $Q_0(l_0)$, we approximate the finger by an infinitely thin line confined to a channel of width W [Fig. 4(d)], and use conformal mapping to derive the corresponding pressure field analytically. Even though the thin-finger approximation will not be an entirely faithful representation of the flow field near the finger, global quantities, such as the total flow focused in the finger, should be represented with good accuracy, as they primarily depend on the length of the finger.

The volumetric flux entering the finger base can be expressed as $Q_0(l_0) = Q_{\text{tot}} f(l_0/W)$ where W is the width of the Hele-Shaw cell. The function $f(\xi)$ can be determined from the pressure field derived in [40], by integrating the leakage flux around the exterior of the finger:

$$f(\xi) = 1 - \frac{2}{\pi}\arctan[\operatorname{csch}(\pi\xi)]. \tag{10}$$

Combining (7), (8) and (10) we get the slope of the finger

$$\frac{\mathrm{d}w}{\mathrm{d}\tilde{x}} = \frac{Dh_{\max}\pi^2}{Q_0(\tilde{x})} = \frac{\pi^2}{\mathrm{Pe}} f(\tilde{x}/W)^{-1}, \tag{11}$$

where $\tilde{x} = x_{\text{tip}} - x$ is the distance from the tip. The shape is then obtained as an integral of (11):

$$w(\tilde{x}) - w_0 = \frac{\pi^2}{\mathrm{Pe}} \int_{x_0}^{\tilde{x}} f(\zeta/W)^{-1}\mathrm{d}\zeta. \tag{12}$$

Since Eq. (11) defines only the slope of the finger, Eq. (12) includes an additional degree of freedom, corresponding to a translation of the entire shape by w_0.

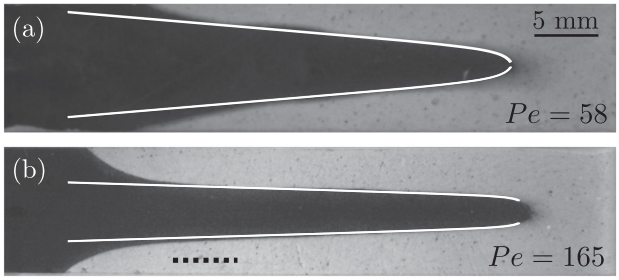

FIG. 5. Experimentally generated dissolution fingers with the theoretically predicted shapes (white) based on Eq. (12). The experimental parameters are (a) $Q_{\text{tot}} = 0.12$ ml/h, $h_0 = 70$ μm and $h_{\max} = 570$ μm, and (b) $Q_{\text{tot}} = 0.16$ ml/h, $h_0 = 70$ μm and $h_{\max} = 270$ μm. The black dashed line indicates the region in which the total flow in the finger can be estimated from the slope.

Additionally, the location of x_{tip} should be adjusted to account for the transition from a finite size finger to the needle shape used in the conformal mapping.

Equation (12) describes the body of the finger, apart from the tip. A comparison of the predicted shape with experimental observations is indicated by the white lines in Fig. 5. However, the same approach cannot be applied in the tip region for two reasons. First, the assumption of a large aspect ratio, $w'(x) \ll 1$, no longer holds near the tip. Second, the separation between reactive and diffusive timescales (and corresponding length scales) no longer holds. Near the tip, the flow becomes focused by the converging boundaries of the finger. The penetration length l_p (Fig. 2) increases due to the higher fluid velocity, and becomes comparable to the radius of curvature of the tip. Hence, a two-phase approximation with a sharp interface is not applicable in this region. Existing models of dissolution finger tips [41,42] assume a sharp interface and therefore depend only on the Péclet number. A proper theory of the tip shape should involve both Péclet and Damköhler numbers and would require resolving the partially dissolved region between the two phases. Such a solution could then be matched with the solution for the body at x_0.

Still, a number of conclusions can be drawn based on Eq. (12) alone. In particular, sufficiently far from the tip, the flow saturates to Q_{tot} with the corresponding slope $w' = \pi^2/\mathrm{Pe}$. This suggests the possibility of deducing the flow rate in the finger from its shape. Such measurements should be taken as far from the tip as possible but not too close to the base, where concave inlet structures connecting the finger to the system edges become noticeable. A suitable location is indicated by the black dashed line in Fig. 5(b).

The model can also be employed to understand the dynamics of interacting fingers. The key lies in Eq. (9), which shows that to maintain the invariance of the finger, the flow through any cross section comoving with the tip must be kept constant. When a finger wins the competition, and the flow through its base (Q_0) increases, it is easy to

meet the invariant flow condition by redirecting part of the excess flow to the sides of the finger. As for the shorter finger, since it is losing the competition, the flow entering its base decreases, making it impossible to maintain the same flow rates in its body. Lower flows result in higher slopes of the finger sides [cf. Eq. (11)], causing the finger to become more bulky with time.

To interpret natural forms, such as the solution pipes shown in Fig. 1, we must consider three spatial dimensions. Here, the invariance condition gives an equation for the radius of the pipe $a(x)$ as a function of volumetric flow rate through the cross section (see SM, Sec. IV [31]):

$$\frac{\mathrm{d}a}{\mathrm{d}x} = -\frac{\pi a D}{2Q}(j_{0,1})^2, \tag{13}$$

where $j_{0,1}$ is the first zero of the Bessel function J_0. From this equation, we can estimate the flow in natural fingers, as described earlier.

Taking as an example the solution pipe in Fig. 1(a), the slope of the sides, $\mathrm{d}a/\mathrm{d}x$ is about $1/10$, which gives the characteristic Péclet number, $\mathrm{Pe} = Q/Da \approx 100$. Taking the diffusion constant of calcium ions as $D = 10^{-5}$ cm^2/s and the pipe radius $a \approx 30$ cm gives an average velocity of about 10^{-5} cm/s, which is a reasonable value [43], given the high porosity and permeability of the underlying rocks [44].

In practice we rarely encounter fingers in isolation or in pairs; instead, we observe an entire group, as depicted in SM, Fig. S1 (microfluidic experiment) or Fig. S3 (natural forms). For the finger to keep its shape, we need only to ensure that the volumetric flow to the base of a given finger does not decrease over time. This can be easily achieved if the finger locally outcompetes its neighbors. Therefore, we can identify the fingers that are locally the longest (e.g., in Fig. S1C, there are five such fingers), measure their slopes, and average the results over the group.

In this Letter, we have summarized experimental results showing that an individual dissolution finger emerges with a shape that is invariant from its inception. This is different from the classical Saffman-Taylor finger, which only obtains its invariant shape at long times. We presented an analysis, based on reactive-transport theory, that allowed us to describe this invariant shape. Field measurements of the slope of the solution pipe allow us to estimate the flow in natural fingers during their formation. This may provide information about the environmental conditions under which they developed.

Acknowledgments—This work was supported by the National Science Centre (NCN; Poland) under CEUS-UNISONO Grant No. 2020/02/Y/ST3/00121. The work of A. L. was supported by the U.S. Department of Energy, Office of Science, Office of Basic Energy Sciences, Geosciences program under Award No. DE-SC0018676. We thank C. Josserand, M. Lipar, K. Mizerski, J. Piasecki, and Y. Pomeau for helpful discussions. We gratefully acknowledge the help of Prof. Piotr Garstecki group (Institute of Physical Chemistry, Polish Academy of Sciences) in setting up the microfluidic experiments.

[1] P. J. Ortoleva, *Geochemical Self-Organization* (Oxford University Press, New York, 1994).
[2] B. Jamtveit and P. Meakin, *Growth, Dissolution and Pattern Formation in Geosystems* (Springer, New York, 1999).
[3] B. Jamtveit and O. Hammer, Sculpting of rocks by reactive fluids, Geochem. Perspect. **1**, 341 (2012).
[4] A. P. Petroff, O. Devauchelle, D. M. Abrams, A. E. Lobkovsky, A. Kudrolli, and D. H. Rothman, Geometry of valley growth, J. Fluid Mech. **673**, 245 (2011).
[5] L. Ristroph, M. N. Moore, S. Childress, M. J. Shelley, and J. Zhang, Sculpting of an erodible body by flowing water, Proc. Natl. Acad. Sci. U.S.A. **109**, 19606 (2012).
[6] B. D. Quaife and M. N. J. Moore, A boundary-integral framework to simulate viscous erosion of a porous medium, J. Comput. Phys. **375**, 1 (2018).
[7] D. J. Jerolmack and K. E. Daniels, Viewing Earth's surface as a soft-matter landscape, Nat. Rev. Phys. **1**, 716 (2019).
[8] W. Dreybrodt, The role of dissolution kinetics in the development of karst aquifers in limestone: A model simulation of karst evolution, J. Geol. **98**, 639 (1990).
[9] A. Ginés, M. Knez, T. Slabe, and W. Dreybrodt, *Karst Rock Features. Karren Sculpturing: Karren Sculpturing* (Založba ZRC, 2009), Vol. 9.
[10] P. Szymczak and A. J. C. Ladd, The initial stages of cave formation: Beyond the one-dimensional paradigm, Earth Planet. Sci. Lett. **301**, 424 (2011).
[11] A. Guérin, J. Derr, S. Courrech Du Pont, and M. Berhanu, Streamwise dissolution patterns created by a flowing water film, Phys. Rev. Lett. **125**, 194502 (2020).
[12] J. M. Huang, J. Tong, M. Shelley, and L. Ristroph, Ultra-sharp pinnacles sculpted by natural convective dissolution, Proc. Natl. Acad. Sci. U.S.A. **117**, 23339 (2020).
[13] J. De Waele, S.-E. Lauritzen, and M. Parise, On the formation of dissolution pipes in quaternary coastal calcareous arenites in mediterranean settings, Earth Surf. Processes Landforms **36**, 143 (2011).
[14] M. Lipar, P. Szymczak, S. Q. White, and J. A. Webb, Solution pipes and focused vertical water flow: Geomorphology and modelling, Earth-Sci. Rev. **218**, 103635 (2021).
[15] P. Meakin, *Fractals, Scaling and Growth Far From Equilibrium* (Cambridge University Press, Cambridge, England, 1998).
[16] P. Pelcé, *New Visions on Form and Growth: Fingered Growth, Dendrites, and Flames* (Oxford University Press, New York, 2004).
[17] P. G. Saffman and G. Taylor, The penetration of a fluid into a porous medium or Hele-Shaw cell containing a more viscous liquid, Proc. R. Soc. A **245**, 312 (1958).
[18] G. Ivantsov, The temperature field around a spherical, cylindrical, or pointed crystal growing in a cooling solution, Dokl. Akad. Nauk SSSR **58**, 567 (1947).

[19] Y. B. Zeldovich, A. G. Istrtov, N. I. Kidin, and V. B. Librovich, Flame propagation in tubes: Hydrodynamics and stability, J. Cryst. Growth **24**, 1 (1980).
[20] P. Pelce and A. Pumir, Cell shape in directional solidification in the small Péclet number limit, J. Cryst. Growth **73**, 337 (1985).
[21] M. B. Short, J. C. Baygents, J. W. Beck, D. A. Stone, R. S. Toomey III, and R. E. Goldstein, Stalactite growth as a free-boundary problem: A geometric law and its platonic ideal, Phys. Rev. Lett. **94**, 018501 (2005).
[22] M. B. Short, J. C. Baygents, and R. E. Goldstein, A free-boundary theory for the shape of the ideal dripping icicle, Phys. Fluids **18**, 083101 (2006).
[23] A. S.-H. Chen and S. W. Morris, Experiments on the morphology of icicles, Phys. Rev. E **83**, 026307 (2011).
[24] J. Mac Huang and N. J. Moore, Morphological attractors in natural convective dissolution, Phys. Rev. Lett. **128**, 024501 (2022).
[25] N. Goldenfeld, P. Y. Chan, and J. Veysey, Dynamics of precipitation pattern formation at geothermal hot springs, Phys. Rev. Lett. **96**, 254501 (2006).
[26] D. Chadam, P. Ortoleva, and A. Sen, A weakly nonlinear stability analysis of the reactive infiltration interface, SIAM J. Appl. Math. **48**, 1362 (1988).
[27] P. Szymczak and A. J. C. Ladd, Reactive-infiltration instabilities in rocks. Fracture dissolution, J. Fluid Mech. **702**, 239 (2012).
[28] J. Krug, K. Kessner, P. Meakin, and F. Family, Laplacian needle growth, Europhys. Lett. **24**, 527 (1993).
[29] J. Krug, Origin of scale invariance in growth processes, Adv. Phys. **46**, 139 (1997).
[30] Y. Cabeza, J. J. Hidalgo, and J. Carrera, Competition is the underlying mechanism controlling viscous fingering and wormhole growth, Geophys. Res. Lett. **47**, e2019GL08479 (2020).
[31] See Supplemental Material at http://link.aps.org/supplemental/10.1103/PhysRevLett.134.094101 for derivations, which includes Refs. [32–37].
[32] F. Osselin, A. Budek, O. Cybulski, P. Kondratiuk, G. P., and P. Szymczak, Microfluidic observation of the onset of reactive in infiltration instability in an analog fracture, Geophys. Res. Lett. **43**, 6907 (2016).
[33] J. Colombani, Measurement of the pure dissolution rate constant of a mineral in water, Geochim. Cosmochim. Acta **72**, 5634 (2008).
[34] L. N. Plummer, T. L. M. Wigley, and D. L. Parkhurst, The kinetics of calcite dissolution in CO_2-water systems at 5°C to 60°C and 0.0 to 1.0 atm of CO_2, Am. J. Sci. **278**, 179 (1978).
[35] F. Dutka, V. Starchenko, F. Osselin, S. Magni, P. Szymczak, and A. J. C. Ladd, Time-dependent shapes of a dissolving mineral grain: Comparisons of simulations with microfluidic experiments, Chem. Geol. **540**, 119459 (2020).
[36] A. J. C. Ladd and P. Szymczak, Use and misuse of large-density asymptotics in the reaction-infiltration instability, Water Resour. Res. **53**, 2419 (2017).
[37] V. Balakotaiah, Hyperbolic averaged models for describing dispersion effects in chromatographs and reactors, Korean J. Chem. Eng. **21**, 318 (2004).
[38] R. Bird, W. Stewart, and E. Lightfoot, *Transport Phenomena* (John Wiley, New York, 2002).
[39] Y. Muzychka, E. Walsh, and P. Walsh, Simple models for laminar thermally developing slug flow in noncircular ducts and channels, J. Heat Transfer **132**, 111702 (2010).
[40] T. Gubiec and P. Szymczak, Fingered growth in channel geometry: A Loewner-equation approach, Phys. Rev. E **77**, 041602 (2008).
[41] R. H. Nilson and S. K. Griffiths, Wormhole growth in soluble porous materials, Phys. Rev. Lett. **65**, 1583 (1990).
[42] P. Kondratiuk and P. Szymczak, Steadily translating parabolic dissolution fingers, SIAM J. Appl. Math. **75**, 2193 (2015).
[43] S. Earle, *Physical Geology* (BCcampus, 2019).
[44] R. P. Sharma, M. Białecki, M. P. Cooper, A. P. Radliński, and P. Szymczak, Pore merging and flow focusing: Comparative study of undissolved and karstified limestone based on microtomography, Chem. Geol. **627**, 121397 (2023).